

Title: Mechanism of signal sequence handover from NAC to SRP on ribosomes during ER-protein targeting

Ahmad Jomaa^{1†}, Martin Gamberdinger^{2†}, Hao-Hsuan Hsieh^{3†}, Annalena Wallisch², Viswanathan
5 Chandrasekaran⁴, Zeynel Ulusoy², Alain Scaiola¹, Ramanujan S. Hegde⁴, Shu-ou Shan^{3*}, Nenad
Ban^{1*}, Elke Deuerling^{2*}

Affiliations:

¹Department of Biology, Institute of Molecular Biology and Biophysics, ETH Zurich, 8093

10 Zurich, Switzerland

²Department of Biology, Molecular Microbiology, University of Konstanz, 78457

Konstanz, Germany

³Division of Chemistry and Chemical Engineering, California Institute of Technology,

Pasadena, CA, 91125, USA

15 ⁴MRC Laboratory of Molecular Biology, Cambridge, UK.

* Correspondence to: elke.deuerling@uni-konstanz.de; ban@mol.biol.ethz.ch;

sshantech.edu

20 [†] These authors contributed equally to this work

Abstract:

The nascent polypeptide-associated complex (NAC) interacts with newly synthesized proteins at the ribosomal tunnel exit. NAC competes with the signal recognition particle (SRP) to prevent mistargeting of cytosolic and mitochondrial polypeptides to the endoplasmic reticulum (ER). How NAC antagonizes SRP and how this is overcome by ER targeting signals is unknown. Here, we found that NAC uses two domains with opposing effects to control SRP access. The core globular domain prevented SRP from binding to signal-less ribosomes, whereas a flexibly attached domain transiently captured SRP to permit scanning of nascent chains. The emergence of an ER targeting signal destabilized NAC's globular domain and facilitated SRP access to the nascent chain. These findings elucidate how NAC hands over the signal sequence to SRP and imparts specificity of protein localization.

One-Sentence Summary: The nascent polypeptide-associated complex regulates signal recognition particle function and controls endoplasmic reticulum targeting.

Main Text

Localization of nascent proteins to the appropriate organelle is essential for cell function and homeostasis. The accuracy of co-translational targeting to the endoplasmic reticulum (ER) relies on two ribosome-binding factors. Signal recognition particle (SRP) uses its M-domain to engage hydrophobic ER targeting signals as they emerge from the ribosomal tunnel and delivers the ribosome-nascent chain complex (RNC) to the SRP receptor (SR) at the ER membrane using its NG-domain(1–4). SRP is far less abundant than ribosomes in the cell and has high affinity for all ribosomes. Thus, its access must be regulated to selectively target ribosomes displaying the ER signal sequence (5, 6). The nascent polypeptide-associated complex (NAC) (composed of NAC α and NAC β) prevents SRP from promiscuously targeting ribosomes without an ER targeting signal(7–11). NAC $\alpha\beta$ consists of a central globular domain from which flexible N- and C-terminal tails extend(12–14). Crosslinking studies have suggested that the N-terminal tails are used for a range of interactions and participate in ribosome binding(15, 16). The function of the C-terminal tails including a conserved ubiquitin-associated domain (UBA) in NAC α , are unknown. NAC and SRP share overlapping ribosome binding sites, which may give rise to their antagonism(15). However, biochemical experiments showed that NAC and SRP bind simultaneously to RNCs translating ER proteins(8, 10, 11), suggesting there is a handoff intermediate in the poorly understood NAC-to-SRP exchange reaction. Thus, we set out to explain how NAC binds the ribosome to prevent SRP access and how this inhibition is preferentially overcome for ER targeting signals.

Structures of NAC in complex with translating ribosome

We reconstituted in vitro a reaction with signal-containing RNC (RNC_{SS}) mixed with both NAC and SRP and analyzed the complexes formed by cryo-electron microscopy (cryo-EM) (fig. S1). This reaction was likely to contain intermediates at critical steps of cargo recognition and

handover, which could be deconvoluted by in silico classification. To this end, we resolved two complexes within the particles, a pre-cargo handover RNC_{ss}•NAC complex, which we will discuss first, and a ternary post-cargo handover RNC_{ss}•NAC•SRP complex, which is discussed later.

The structure of the RNC_{ss}•NAC complex was similar to the RNC•NAC structure obtained from re-analysis of an RNC intermediate during translation of the cytosolic protein tubulin (TUBB) (fig. S2 and S3), on which NAC co-purified (17). This suggests that NAC initially engages both signal-containing and signal-lacking RNCs, but would be expected to handover to SRP only in the presence of an ER signal sequence.

The structure of the RNC_{ss}•NAC complex (Fig. 1A-D; G) revealed the interactions between the N-terminal tail of NAC β and the ribosome at 3.5 Å resolution (Fig. 1C, fig. S4). The tail, containing an RRKKK motif, forms an α -helix followed by a loop in an anchor-shaped turn wrapping around eL22 while also contacting eL19 and the ribosomal RNA (rRNA) (Fig. 1C, fig. S4). The structure rationalizes the key role of this domain in ribosome binding established previously (15, 18, 16). To validate the role of this tail as an anchor to the ribosome, we measured NAC-ribosome binding affinity using Förster resonance energy transfer (FRET) between a donor dye placed near the signal sequence on the nascent chain and an acceptor dye placed on NAC. Point mutations of the NAC tail weakened NAC-RNC binding by 10-40-fold (Fig. 1E-F), consistent with its important role in ribosome binding.

The globular domain of NAC was resolved to approximately 8 Å resolution, which allowed rigid body fitting of an Alphafold predicted structure (19) (Fig. 1A-B, fig. S5). Based on this interpretation, two positively charged α -helices contributed by both NAC subunits contact rRNA on the surface of the ribosome (Fig. 1G, fig. S5). Charge reversal mutations of a positively charged residue in each helix (K78E-NAC α or K43E-NAC β) weakened ribosome binding of NAC in vitro (fig. S6A) and in vivo (fig. S6B).

The binding site of NAC globular domain overlaps with that of SRP M-domain and is mutually exclusive with SRP binding (Fig. 1G and fig. S6C) (3, 4), consistent with a low-resolution cryo-EM map of NAC in complex with inactive ribosomes (15). This finding suggests that NAC interaction at the ribosome exit site is the basis of SRP inhibition. In agreement with this hypothesis, a ribosome binding mutant in the globular domain (K78E-NAC α combined with K43E-NAC β , termed NAC KK-EE) was impaired in its ability to compete with SRP binding in vitro (Fig. 1H). The residual binding of NAC KK-EE to the ribosome is likely mediated by the N-terminus of NAC β , the position of which would not interfere with SRP binding (fig. S6C).

The corresponding NAC KK-EE mutations in *C. elegans* showed reduced competition of SRP binding by NAC as judged by elevated levels of ribosome-bound SRP (Fig. 1I, fig. S6D) as well as increased recovery of mRNAs coding for non-ER proteins in SRP pulldowns (fig. S6E). The reduction in SRP competition correlated with elevated levels of a GFP reporter of ER stress driven by the hsp-4 promoter (hsp-4p::GFP) (20), particularly in highly secretory intestinal cells (fig. S6F). Moreover, worms expressing mutant NAC showed reduced embryonic viability (fig. S6G) and a shortened adult lifespan (fig. S6H).

NAC is destabilized by ER signal sequences allowing access of SRP to the ribosome exit

SRP antagonism by NAC must be relieved when an ER targeting signal emerges from the ribosome. One possibility is that hydrophobic ER targeting signals somehow weaken the interaction between the NAC globular domain and the ribosome to allow SRP access. To test this, we compared the affinity of NAC for RNCs displaying either an ER signal sequence (RNC_{SS}) or a mutated signal sequence that inhibits ER targeting (RNC_{SSmt}) (fig. S7) (21). Since the NAC β anchor tail would mask the affinity differences, we performed FRET measurements with NAC mutants with a disrupted RRKKK motif. These mutants, NAC-R27A and NAC-K29A, bound to

RNC_{SSmt} with ~3.5-fold and ~5-fold weaker affinity, respectively, compared to RNC_{SS} (fig. S8A and B).

We then measured NAC binding to purified RNCs bearing ER, cytosolic and mitochondrial nascent chains (HSPA5, GPI and HSPD1, respectively) stalled at residue 60, exposing short N-terminal sequences (~30 aa) at the tunnel exit (fig. S7). In agreement with our hypothesis, NAC R27A binds 5-fold more weakly to RNC_{HSPA5} exposing an ER signal sequence than to RNC_{GPI} and RNC_{HSPD1} (Fig. 1J and fig. S8C-D).

We repeated the binding measurements with purified RNCs bearing an ER signal sequence at nascent chain lengths of 30, 40 and 60 aa (Fig. 1J, fig. S8C-D). NAC showed the strongest interaction with ribosome when the signal sequence is in the tunnel (30 and 40 aa), and binding is weakened more than 10-fold when the ER signal peptide is exposed (60 aa). Thus, the emergence of a hydrophobic signal peptide, but not another type of nascent chain, weakens the interaction of NAC globular domain with the ribosome.

We then investigated the role of the two ribosome-binding antiparallel helices that dock the globular domain on the ribosome in proximity to the emerging nascent chain. The helices are amphipathic and orient the positively charged side toward the ribosome surface, whereas the hydrophobic side contributes to a buried hydrophobic pocket (fig. S5). These helices were sensitive to proteolysis when human NAC was subjected to crystallization(13), suggesting that they are flexibly disposed in solution, but are apparently stabilized in the ribosome-bound state. To test this, we engineered two cysteines in the helices such that they would be apposed to each other in the ribosome-bound NAC structure. Consistent with our hypothesis, the engineered cysteines form a disulfide bond after oxidant treatment only in the presence of the ribosome (Fig. 2A and fig. S9).

To investigate whether the emergence of the signaling peptides may destabilize and release the globular domain of NAC from the ribosome (Fig. 2B), we incorporated photo-crosslinking

probes at six positions on NAC. The probes were placed both inside and outside the two interacting helices (Fig. 2B), and then we tested their proximity to nascent chains coding for a cytosolic, mitochondrial, or an ER protein. NAC variants carrying the probe within the hydrophobic pocket (e.g., NAC α -I121) crosslinked to ER targeting signals (Fig. 2C and fig. S10A-C). Crosslinking was dependent on nascent chain length and only seen once the targeting signal was fully exposed outside the exit tunnel (fig. S10A). Crosslinking was prevented when the helices were covalently linked by disulfide bond formation, demonstrating that destabilization of the NAC globular domain by the ER signal peptide requires separation of the helices (Fig. 2D). Furthermore, crosslinking to the pocket residues NAC α -I121 and NAC β -L48, but not the less buried NAC α -M80, was modulated by changing targeting signal hydrophobicity (fig. S10D). Mutating M80 to serine impaired nascent chain photo-crosslinking to NAC α -I121 (Fig. 2E), which suggests this residue also contributes to nascent chain sensing.

These results indicate that an ER signal sequence destabilizes the NAC globular domain. The NAC β N-terminal tail remains anchored to the ribosomal surface regardless of the nascent chain, as evidenced by crosslinking between a residue in the NAC β anchor and the ribosomal protein eL22, whereas a probe in the N-terminus of NAC α changed its location only for the ER substrate (fig. S11). Combined, these results suggest that NAC interactions with the ribosome are remodeled as the signal peptide emerges from the ribosome tunnel.

Flexibly tethered UBA domain of NAC recruits SRP

The cryo-EM data on RNC_{ss} mixed with both NAC and SRP also allowed us to visualize the complex with NAC and SRP simultaneously bound to the ribosome (RNC_{ss}•NAC•SRP) (Fig. 3A, fig. S1 and S12). The conformation of SRP in the ternary complex was similar to previously observed SRP-ribosome complexes (3, 4). The density for the NAC β anchor was observed in a similar position as in the RNC•NAC complexes (fig. S12C). However, the globular domain of

NAC is no longer resolved, because its binding position at the tunnel exit is occupied by the SRP54 M-domain (Fig. 3A-D and Fig. 1G).

In addition, we observed density for the flexibly tethered C-terminal UBA domain of NAC α bound to the N-domain of SRP54 (Fig. 3B-C, fig. S12 and S13). The interactions occupy two patches of contact points and involve a number of salt bridges and specific hydrogen bonds between highly conserved residues (Fig. 3C-D, fig. S14). The UBA binding site on SRP54 overlaps with the binding site of the NG-domain of SR (fig. S15), which suggests that formation of the SRP•SR complex will displace NAC from SRP at the ER membrane (22–24). The direct interaction of the UBA domain of NAC with SRP raises questions as to whether it plays a role in ER targeting.

To address this, we generated: (i) a NAC mutant in which the UBA is deleted (dUBA), (ii) NAC mutant (D205R/N208R-NAC α , termed UBAm α), and (iii) SRP mutant (K50E/R53E-SRP54, termed SRP54mt based on human sequence numbering). UBAm α and SRP54mt contain charge reversal mutations at contact points between the UBA and the NG-domain of SRP54. We measured the effects of these mutations on the binding affinity of SRP for NAC-engaged RNC_{ss} displaying the ER signal sequence. Although none of the above-described mutations changed the affinity of NAC or SRP for SR or RNCs (fig. S16 and S17B-C), they all decreased the affinity of SRP for the RNC_{ss}•NAC complex by more than 5-fold (Fig. 3E and fig. S17A). The same effect was observed in reciprocal experiments when NAC was titrated to a pre-formed RNC_{ss}•SRP complex (fig. S17B-C). Thus, the contact between NAC UBA and SRP54 NG-domains stabilizes the co-binding of SRP and NAC on signal sequence-displaying ribosomes.

To test whether the UBA domain mediates the initial recruitment of SRP to the ribosome, we used total internal reflection fluorescence (TIRF) microscopy to study single molecule events in which SRP binds to surface-immobilized RNC_{ss} pre-bound with NAC (Fig. 4A). If SRP is

captured by NAC via the UBA domain prior to stable engagement with the ribosome, then the arrival of SRP on NAC-bound RNC_{SS} would be synchronous with the onset of FRET between a dye pair engineered on the SRP54 NG and NAC α UBA domains. The results are consistent with this model: the initiation of co-localized fluorescence signals from NAC and SRP is synchronous with the onset of FRET in every single molecule fluorescence time trace (Fig. 4B and C), even in recruitment events that did not lead to long-lived SRP association with the RNC (example in Fig. 5). Statistical analysis, in which the FRET time traces were aligned to the start of the SRP fluorescence signal (n = 45), showed that peak FRET efficiency was coincident with SRP arrival (Fig. 4D). Once a stable RNC•NAC•SRP ternary complex is formed, NAC α UBA dynamically associates with and dissociates from SRP54, as shown by the frequent transitions between low and 10 high FRET states (Fig. 4E). Thus, the contact between UBA and NG initiates before the productive docking of SRP at the exit of the ribosomal tunnel and signal sequence handover.

15 *C. elegans* mutants with impaired NAC UBA-SRP54 NG interactions showed elevated levels of the ER stress reporter hsp-4p::GFP, particularly in highly secretory intestinal cells (Fig. 3F and fig. S18A, B). Furthermore, the levels of a secreted GFP reporter containing a signal sequence (ssGFP) (25) were significantly lower in NAC UBA and SRP54 NG mutant worms (Fig. 3G and fig. S18C-D). The mutant worms also showed a cytosolic stress response, suggesting a possible accumulation of misfolded ER proteins in the cytosol due to failed targeting (fig. S18E). 20 As mentioned above, the defects observed with SRP54mt was not due to impaired interaction with the SR NG domain (fig. S15 and S16). Thus, the contacts between SRP and the UBA domain of NAC is critical for the successful SRP targeting of proteins to the ER.

Mechanism of the NAC and SRP interplay on the ribosome to initiate ER targeting

We propose a molecular mechanism for the interplay of NAC and SRP at the ribosome that controls and initiates co-translational protein targeting to ER: NAC acts as “gatekeeper” to shield

emerging nascent chains from non-physiological interactions with SRP (Fig. 5). Owing to its abundance and high affinity for the ribosome, NAC is bound to most ribosomes at early stages of translation via a high affinity anchor, and a weakly bound globular domain that blocks SRP access to nascent polypeptides. The flexibly tethered UBA domain recruits SRP and increases its local concentration at the tunnel exit region to initiate sampling of nascent chains. The emergence of an 5 ER signal sequence weakens the interactions of NAC's globular domain with the ribosome. This allows SRP to bind the signal sequence at the exit of the ribosomal tunnel displacing the globular domain of NAC. NAC remains associated with both the ribosome and SRP via the respective NAC β anchor and UBA contacts, until it reaches the ER membrane where SR displaces the UBA 10 domain from SRP.

This study resolves the molecular functions of NAC as a sorting factor for nascent chains and the nature of its spatiotemporal coordination with SRP on the ribosome. It explains how NAC, which binds to virtually all ribosomes, prevents sub-stoichiometric SRP from forming tight but unproductive complexes with signal-less ribosomes, while at the same time keeping SRP anchored 15 to allow it to scan for the presence of the ER signal sequence. Because degenerate and highly diverse targeting sequences cannot be recognized with sufficient specificity in a single step and/or by individual targeting factors, stepwise recognition by NAC followed by SRP, coupled with quality control pathways (26–29), increases the overall fidelity of protein targeting. The exit region of the ribosomal tunnel is a crowded environment where multiple binding factor compete for the 20 nascent chain. Therefore, it is possible that NAC's role as a sorting factor extends beyond the recruitment of SRP to orchestrate a multitude of nascent chain processing events.

References

1. R. Gilmore, G. Blobel, P. Walter, Protein translocation across the endoplasmic reticulum. I. Detection in the microsomal membrane of a receptor for the signal recognition particle. *Journal of Cell Biology*. **95**, 463–469 (1982).
5. 2. M. Halic, M. Blau, T. Becker, T. Mielke, M. R. Pool, K. Wild, I. Sinning, R. Beckmann, Following the signal sequence from ribosomal tunnel exit to signal recognition particle. *Nature*. **444**, 507–511 (2006).
3. 10. R. M. Voorhees, R. S. Hegde, Structures of the scanning and engaged states of the mammalian SRP-ribosome complex. *eLife*. **4** (2015), doi:10.7554/eLife.07975.
4. 15. A. Jomaa, S. Eitzinger, Z. Zhu, S. Chandrasekar, K. Kobayashi, S.-O. Shan, N. Ban, Molecular mechanism of cargo recognition and handover by the mammalian signal recognition particle. *Cell reports*. **36**, 109350 (2021).
5. 20. E. A. Costa, K. Subramanian, J. Nunnari, J. S. Weissman, Defining the physiological role of SRP in protein-targeting efficiency and specificity. *Science*. **359**, 689–692 (2018).
6. 25. M. Gainerdinger, M. A. Hanebuth, T. Frickey, E. Deuerling, The principle of antagonism ensures protein targeting specificity at the endoplasmic reticulum. *Science*. **348**, 201–207 (2015).
7. 30. B. Wiedmann, H. Sakai, T. A. Davis, M. Wiedmann, A protein complex required for signal-sequence-specific sorting and translocation. *Nature*. **370**, 434–440 (1994).
8. 35. M. del Alamo, D. J. Hogan, S. Pechmann, V. Albanese, P. O. Brown, J. Frydman, Defining the Specificity of Cotranslationally Acting Chaperones by Systematic Analysis of mRNAs Associated with Ribosome-Nascent Chain Complexes. *PLoS Biology*. **9**, e1001100 (2011).
9. 40. Y. Nyathi, M. R. Pool, Analysis of the interplay of protein biogenesis factors at the ribosome exit site reveals new role for NAC. *Journal of Cell Biology*. **210**, 287–301 (2015).
10. 45. Y. Zhang, U. Berndt, H. Götz, A. Tais, S. Oellerer, T. Wölfle, E. Fitzke, S. Rospert, NAC functions as a modulator of SRP during the early steps of protein targeting to the endoplasmic reticulum. *Molecular Biology of the Cell*. **23**, 3027–3040 (2012).
11. 50. H.-H. Hsieh, J. H. Lee, S. Chandrasekar, S. Shan, A ribosome-associated chaperone enables substrate triage in a cotranslational protein targeting complex. *Nature Communications*. **11**, 5840 (2020).

12. Y. Liu, Y. Hu, X. Li, L. Niu, M. Teng, The Crystal Structure of the Human Nascent Polypeptide-Associated Complex Domain Reveals a Nucleic Acid-Binding Region on the NACA Subunit,. *Biochemistry*. **49**, 2890–2896 (2010).
- 5 13. L. Wang, W. Zhang, L. Wang, X. C. Zhang, X. Li, Z. Rao, Crystal structures of NAC domains of human nascent polypeptide-associated complex (NAC) and its α NAC subunit. *Protein & Cell*. **1**, 406–416 (2010).
14. T. Spreter, M. Pech, B. Beatrix, The Crystal Structure of Archaeal Nascent Polypeptide-associated Complex (NAC) Reveals a Unique Fold and the Presence of a Ubiquitin-associated Domain. *Journal of Biological Chemistry*. **280**, 15849–15854 (2005).
- 10 15. M. Gämmerdinger, K. Kobayashi, A. Wallisch, S. G. Kreft, C. Sailer, R. Schlömer, N. Sachs, A. Jomaa, F. Stengel, N. Ban, E. Deuerling, Early Scanning of Nascent Polypeptides inside the Ribosomal Tunnel by NAC. *Molecular Cell*. **75**, 996-1006.e8 (2019).
16. R. D. Wegrzyn, D. Hofmann, F. Merz, R. Nikolay, T. Rauch, C. Graf, E. Deuerling, A Conserved Motif Is Prerequisite for the Interaction of NAC with Ribosomal Protein L23 and Nascent Chains. *Journal of Biological Chemistry*. **281**, 2847–2857 (2006).
- 15 17. Z. Lin, I. Gasic, V. Chandrasekaran, N. Peters, S. Shao, T. J. Mitchison, R. S. Hegde, TTC5 mediates autoregulation of tubulin via mRNA degradation. *Science*. **367**, 100–104 (2020).
18. M. Pech, T. Spreter, R. Beckmann, B. Beatrix, Dual binding mode of the nascent polypeptide-associated complex reveals a novel universal adapter site on the ribosome. *Journal of Biological Chemistry*. **285**, 19679–19687 (2010).
- 20 19. J. Jumper, R. Evans, A. Pritzel, T. Green, M. Figurnov, O. Ronneberger, K. Tunyasuvunakool, R. Bates, A. Žídek, A. Potapenko, A. Bridgland, C. Meyer, S. A. A. Kohl, A. J. Ballard, A. Cowie, B. Romera-Paredes, S. Nikolov, R. Jain, J. Adler, T. Back, S. Petersen, D. Reiman, E. Clancy, M. Zielinski, M. Steinegger, M. Pacholska, T. Berghammer, S. Bodenstein, D. Silver, O. Vinyals, A. W. Senior, K. Kavukcuoglu, P. Kohli, D. Hassabis, Highly accurate protein structure prediction with AlphaFold. *Nature*. **596**, 583–589 (2021).
- 25 20. M. Calfon, H. Zeng, F. Urano, J. H. Till, S. R. Hubbard, H. P. Harding, S. G. Clark, D. Ron, IRE1 couples endoplasmic reticulum load to secretory capacity by processing the XBP-1 mRNA. *Nature*. **415**, 92–96 (2002).

21. J. H. Lee, S. Chandrasekar, S. Chung, Y.-H. Hwang Fu, D. Liu, S. Weiss, S. Shan, Sequential activation of human signal recognition particle by the ribosome and signal sequence drives efficient protein targeting. *Proceedings of the National Academy of Sciences*. **115**, E5487–E5496 (2018).
22. K. Kobayashi, A. Jomaa, J. H. Lee, S. Chandrasekar, D. Boehringer, S.-O. Shan, N. Ban, Structure of a prehandover mammalian ribosomal SRP·SRP receptor targeting complex. *Science*. **360**, 323–327 (2018).
- 5 23. K. Wild, G. Bange, D. Motiejunas, J. Kribelbauer, A. Hendricks, B. Segnitz, R. C. Wade, I. Sinning, Structural Basis for Conserved Regulation and Adaptation of the Signal Recognition Particle Targeting Complex. *Journal of Molecular Biology*. **428**, 2880–2897 (2016).
- 10 24. J. H. Lee, A. Jomaa, S. Chung, Y.-H. Hwang Fu, R. Qian, X. Sun, H.-H. Hsieh, S. Chandrasekar, X. Bi, S. Mattei, D. Boehringer, S. Weiss, N. Ban, S. Shan, Receptor compaction and GTPase rearrangement drive SRP-mediated cotranslational protein translocation into the ER. *Science Advances*. **7** (2021), doi:10.1126/sciadv.abg0942.
- 15 25. H. Fares, I. Greenwald, Regulation of endocytosis by CUP-5, the *Caenorhabditis elegans* mucolipin-1 homolog. *Nature Genetics*. **28** (2001), doi:10.1038/88281.
26. Y. Chen, G. K. E. Umanah, N. Dephoure, S. A. Andrabi, S. P. Gygi, T. M. Dawson, V. L. Dawson, J. Rutter, Msp1/ATAD1 maintains mitochondrial function by facilitating the degradation of mislocalized tail-anchored proteins. *The EMBO Journal*. **33**, 1548–1564 (2014).
- 20 27. R. S. Hegde, E. Zavodszky, Recognition and Degradation of Mislocalized Proteins in Health and Disease. *Cold Spring Harbor Perspectives in Biology*. **11**, a033902 (2019).
28. T. Hessa, A. Sharma, M. Mariappan, H. D. Eshleman, E. Gutierrez, R. S. Hegde, Protein targeting and degradation are coupled for elimination of mislocalized proteins. *Nature*. **475**, 394–397 (2011).
29. V. Okreglak, P. Walter, The conserved AAA-ATPase Msp1 confers organelle specificity to tail-anchored proteins. *Proceedings of the National Academy of Sciences*. **111**, 8019–8024 (2014).
30. S. Q. Zheng, E. Palovcak, J.-P. Armache, K. A. Verba, Y. Cheng, D. A. Agard, MotionCor2: anisotropic correction of beam-induced motion for improved cryo-electron microscopy. *Nature Methods*. **14**, 331–332 (2017).
- 25 31. K. Zhang, Gctf: Real-time CTF determination and correction. *Journal of Structural Biology*. **193**, 1–12 (2016).

32. J. Zivanov, T. Nakane, B. O. Forsberg, D. Kimanius, W. J. Hagen, E. Lindahl, S. H. Scheres, New tools for automated high-resolution cryo-EM structure determination in RELION-3. *eLife*. **7** (2018), doi:10.7554/eLife.42166.
- 5 33. L. A. Kelley, S. Mezulis, C. M. Yates, M. N. Wass, M. J. E. Sternberg, The Phyre2 web portal for protein modeling, prediction and analysis. *Nature Protocols*. **10**, 845–858 (2015).
34. P. Emsley, K. Cowtan, *Coot* : model-building tools for molecular graphics. *Acta Crystallographica Section D Biological Crystallography*. **60**, 2126–2132 (2004).
- 10 35. P. D. Adams, P. v. Afonine, G. Bunkóczki, V. B. Chen, I. W. Davis, N. Echols, J. J. Headd, L.-W. Hung, G. J. Kapral, R. W. Grosse-Kunstleve, A. J. McCoy, N. W. Moriarty, R. Oeffner, R. J. Read, D. C. Richardson, J. S. Richardson, T. C. Terwilliger, P. H. Zwart, *PHENIX*: a comprehensive Python-based system for macromolecular structure solution. *Acta Crystallographica Section D Biological Crystallography*. **66**, 213–221 (2010).
- 15 36. E. F. Pettersen, T. D. Goddard, C. C. Huang, G. S. Couch, D. M. Greenblatt, E. C. Meng, T. E. Ferrin, UCSF Chimera: A visualization system for exploratory research and analysis. *Journal of Computational Chemistry*. **25**, 1605–1612 (2004).
37. T. D. Goddard, C. C. Huang, E. C. Meng, E. F. Pettersen, G. S. Couch, J. H. Morris, T. E. Ferrin, UCSF ChimeraX: Meeting modern challenges in visualization and analysis. *Protein Science*. **27**, 14–25 (2018).
- 20 38. S. Brenner, THE GENETICS OF *CAENORHABDITIS ELEGANS*. *Genetics*. **77**, 71–94 (1974).
39. C. Mello, A. Fire, in *Methods in Cell Biology* (1995; <https://linkinghub.elsevier.com/retrieve/pii/S0091679X08613990>), vol. 48, pp. 451–482.
- 25 40. C. Frøkjær-Jensen, M. W. Davis, M. Sarov, J. Taylor, S. Flibotte, M. LaBella, A. Pozniakovsky, D. G. Moerman, E. M. Jorgensen, Random and targeted transgene insertion in *Caenorhabditis elegans* using a modified Mos1 transposon. *Nature Methods*. **11**, 529–534 (2014).
41. S. Redemann, S. Schloissnig, S. Ernst, A. Pozniakovsky, S. Ayloo, A. A. Hyman, H. Bringmann, Codon adaptation-based control of protein expression in *C. elegans*. *Nature Methods*. **8**, 250–252 (2011).
42. H. Fares, I. Greenwald, Genetic Analysis of Endocytosis in *Caenorhabditis elegans* : Coelomocyte Uptake Defective Mutants. *Genetics*. **159**, 133–145 (2001).

Acknowledgements: We thank M. Leibundgut, T. Lenarcic, and M. Jaskolowski for discussions.

Cryo-EM data was collected at ScopeM at the ETH Zurich. We thank R. Schloemer and E. Coellen for technical assistance, and S. Kreft for help with in vitro cysteine crosslinking experiments, and the *Caenorhabditis Genetics Center* for strains. We acknowledge the support of

5

NVIDIA Corporation for the Titan Xp GPU through a grant program awarded to A.J. **Funding:** This work was supported by the Swiss National Science Foundation (grant number 310030B_163478),

National Center of Excellence in Research RNA & Disease Program of the SNSF (grant number 51NF40_141735), and in part by the Roessler Prize, Ernst Jung Prize, and Otto Naegeli Prize for

Medical Research to N.B., by research grants from the German Science Foundation (SFB969/A01 and A07) to E.D. and M.G., by the National Institutes of Health grant R35 GM136321 and National

10 Science Foundation grant MCB-1929452 to S.-o.S., and by UK Medical Research Council grant MC_UP_A022_1007 (R.S.H.). V.C. was supported by V. Ramakrishnan whose funding was from

the MRC (MC_U105184332), the Wellcome Trust (WT096570), the Agouron Institute, and the Louis-Jeantet Foundation. **Author contributions:** A.J., M.G., H.H., R.S.H., S.-o.S., N.B., and

15 E.D. conceived the project. A.J. and A.S. performed cryo-EM data collection for ER targeting complexes containing NAC and SRP. A.J. determined the cryo-EM structures of NAC-RNC and

NAC-SRP-RNC. M.G., A.W. performed *C. elegans* in vivo and crosslinking experiments. H.H. performed FRET titrations and single molecule experiments. V.C. performed structural analysis

of the NAC-TTC5-RNC. Z.U. characterized NAC cysteine variants. A.J., M.G., H.H., and S.-o.S.,

20 E.D., and N.B. wrote the manuscript. All authors contributed to data analysis and the final version of the manuscript. **Competing interests:** The authors declare no competing interests. **Data and**

materials availability: Cryo-EM maps and model coordinates are deposited in the EMDB as EMD-XXXX, -XXXX, and -XXXX in the PDB as PDB ID YYY, and YYY. All other data are

available in the main text or the supplementary materials

Supplementary Materials

Materials and Methods

5 Figs. S1 to S18

Tables S1 to S3

References (29–42)

Figures

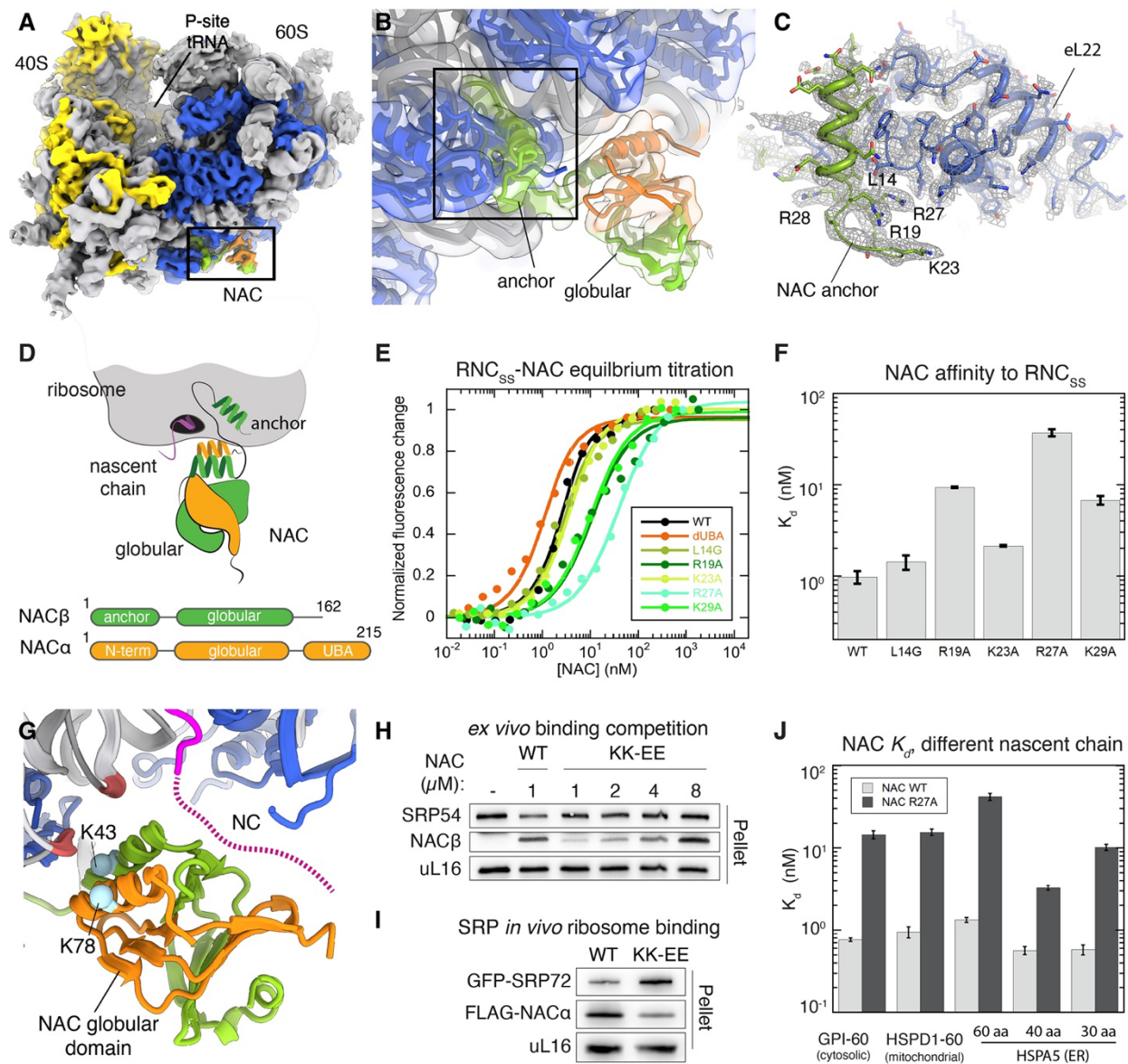


Fig. 1. Structure of the ribosome•NAC complex reveals interactions between NAC globular and anchor domain with the nascent chain and the ribosome. (A) Cryo-EM structure of the RNCss•NAC complex, boxed region indicates the close-up region shown in panel B. (B) A closeup on the ribosome tunnel exit region. NAC β is colored green and NAC α is colored orange. Anchor and globular domains of NAC are indicated. (C) Closeups on the N-terminus of NAC β fitted into

cryo-EM densities shown as mesh. Ribosomal proteins eL22 is shown as blue cartoon ribbon. **(D)** Schematic of the RNC•NAC complex with a domain structure of NAC. **(E)** Equilibrium titrations to measure the binding of the indicated NAC mutants to RNC_{ss}. The fluorescence signal changes were normalized to the end point of each titration for comparison. The lines are fits of the data to Eq 2. **(F)** Summary of the K_d values from panel E. **(G)** Closeup of the NAC globular domain highlighting the two antiparallel α -helices, with residues K78 (NAC α) and K43 (NAC β) shown as spheres (blue) interacting with the backbone of the rRNA (red). Dashed line indicates flexible nascent chain (NC, magenta). **(H)** Crude cellular RNCs were incubated with purified NAC proteins and pelleted by sucrose cushion centrifugation. Proteins were detected by immunoblotting. **(I)** Sucrose cushion centrifugation of ribosomes in *C. elegans* expressing indicated NAC variants and GFP-tagged SRP72. Proteins in the pellet fraction were detected by immunoblotting. **(J)** Summary of the K_d values of NAC R27A for RNCs displaying the nascent chains of GPI (cytosolic), HSPD1 (mitochondrial) and HSPA5 (ER) at the indicated nascent chain lengths. K_d values were from analysis of the data in fig. S8C-D. Error bars are covariances of the fitted K_d values.

15

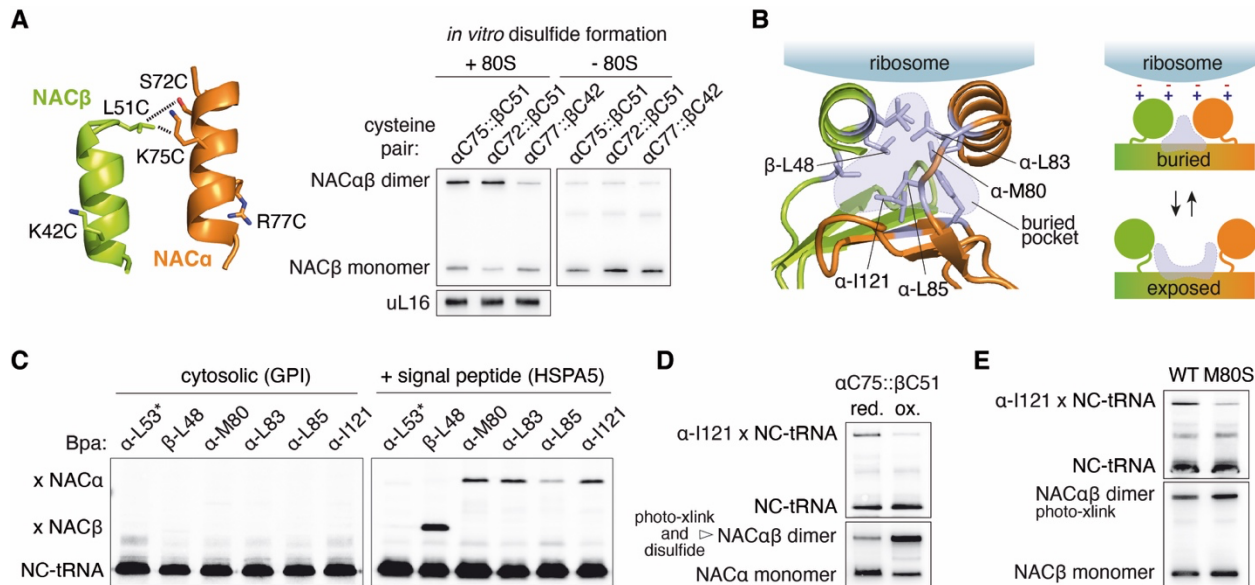


Fig. 2. ER signal sequences are sensed by the ribosome-binding helices of NAC. (A) NAC's ribosome binding helices showing the positions of pairwise cysteine mutants tested for disulfide bond formation. Side chains shown are based on Alphafold prediction. Dashed lines indicate pairs sufficiently close to form a disulfide bond revealed by immunoblotting (right panel) in the presence of inactive 80S ribosomes. **(B)** Residues contributing to the hydrophobic pocket between the two α -helices of NAC (purple). The right side shows a model where ribosome dissociation leads to separation of the helices thereby exposing a hydrophobic pocket. **(C)** Autoradiograph of photo-crosslinking of Bpa-NAC variants to stalled RNCs carrying 50 aa S^{35} -labeled nascent chains of cytosolic GPI (left) or a GPI fusion protein containing the N-terminal signal peptide of HSPA5 (right). The positions of the tRNA-attached nascent chain (NC-tRNA) and its crosslinks to NAC α and NAC β are indicated. Asterisk indicates a position outside the hydrophobic region. **(D)** Autoradiograph of photo-crosslinking of α C75-βC51 cysteine variant carrying Bpa at α -I121 to HSPA5-RNCs (55 aa), performed in the reduced (red.) and oxidized (ox.) state. **(E)** Autoradiograph and immunoblotting of 55 aa HSPA5-RNCs photo-crosslinking of indicated α -I121 Bpa-NAC variants.

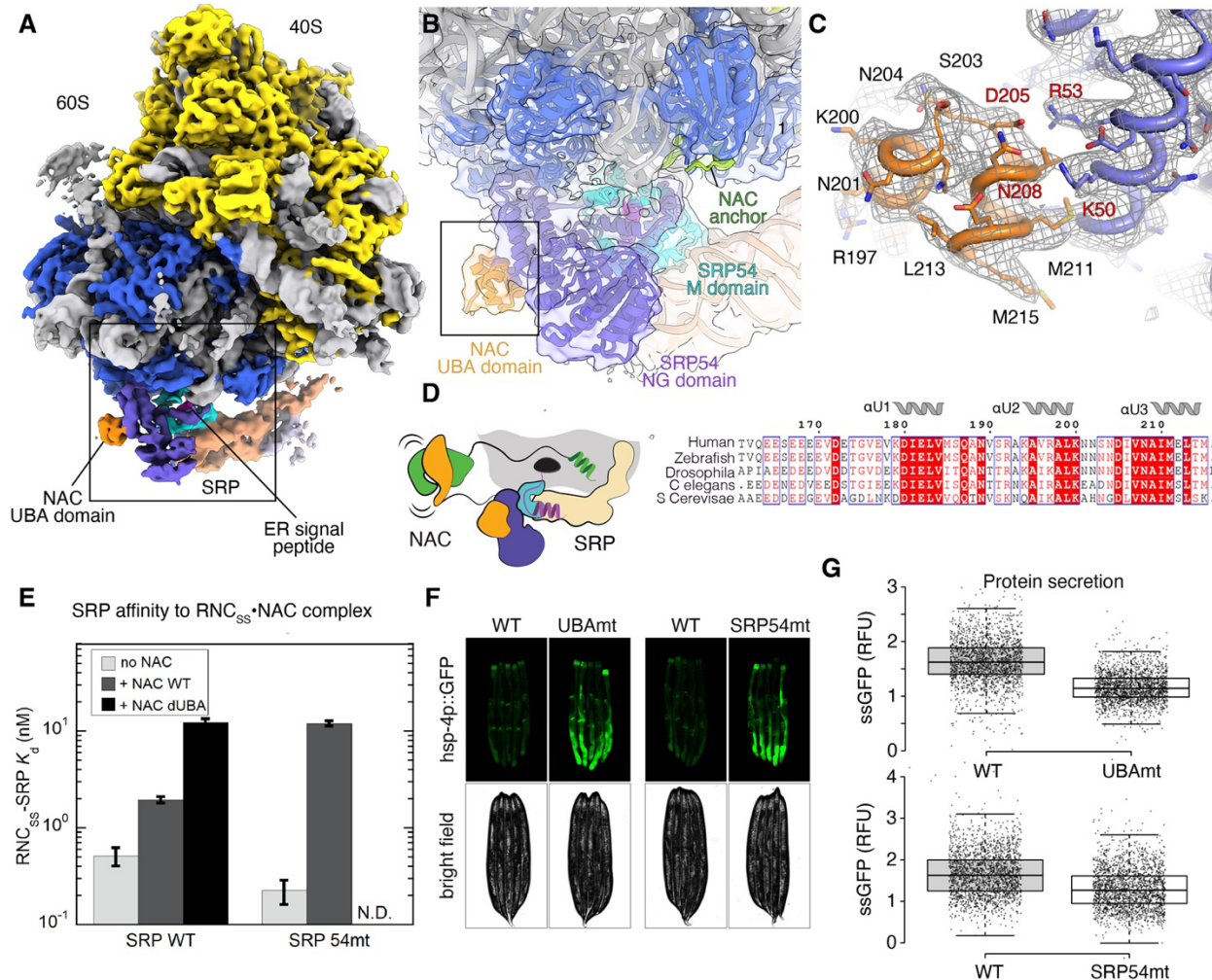


Fig. 3. Structure of the ribosome•SRP•NAC complex. (A) Cryo-EM structure of the RNC_{ss}•NAC•SRP complex, boxed region indicates the close-up shown in panel B. **(B)** Ribosome tunnel exit region depicting SRP54 NG and M domains, NAC_α UBA domain, and NAC_β anchor domain colored slate, cyan, orange, and green, respectively. Underlying EM-density is shown as transparent surface. **(C)** Closeups on the UBA interactions with SRP54 NG domain shown as cartoon and sticks, fitted into cryo-EM densities shown as mesh. **(D)** Schematic representation of the ternary complex. Boxed region shows sequence alignment of NAC_α UBA domain in eukaryotes. **(E)** Summary of the K_d values for the binding of wildtype and mutant SRPs to

5

10

RNCss•NAC, based on fitting of the data in figure S17A. N.D. not determined. **(F)** and **(G)** Fluorescence microscope images of hsp-4p::GFP worms **(F)** and worm flow cytometry analysis of ssGFP **(G)** in worms carrying indicated RNAi-resistant genes in the endogenous RNAi background. Box plot center line = median; box length = upper + lower quartile; whiskers = minimum/maximum quartile; $N \geq 2000$.

5

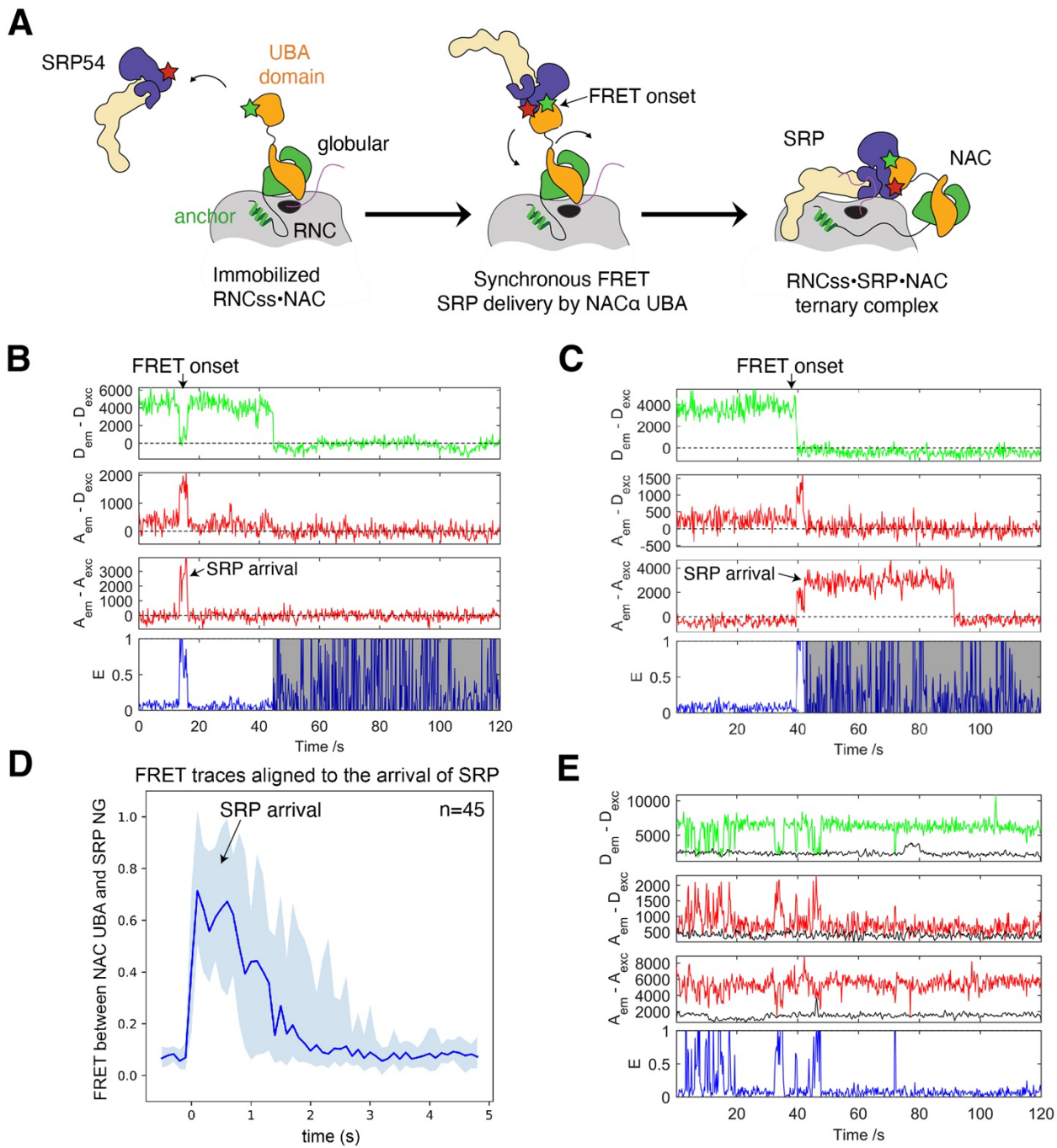


Fig. 4. Interaction between SRP54 and NAC α UBA domain mediates initial SRP recruitment to the ribosome. (A) Scheme of the single molecule experiment. RNC is immobilized on the glass coverslip surface via 3' biotinylated mRNA (not shown). NAC was labeled with Cy3b (green star) in the UBA domain, and SRP is labeled with Atto647N (red star) in the SRP54 NG domain. (B) and (C) Representative single molecule fluorescence time traces. $D_{em} - D_{exc}$, donor emission during

donor excitation. $A_{\text{em}}-D_{\text{ex}}$, acceptor emission during donor excitation. $A_{\text{em}}-A_{\text{ex}}$, acceptor emission during acceptor excitation. E, apparent FRET efficiency, calculated from the $A_{\text{em}}-D_{\text{ex}}$ and $D_{\text{em}}-D_{\text{ex}}$ traces. The region after donor photobleaching is masked. **(D)** Time traces of FRET efficiency (n = 45) are aligned to the start of the SRP (acceptor) signal. The median FRET value of all traces at each time frame is plotted as solid blue line. The blue shaded area encloses the FRET range that includes the first to third quartile of data at each frame. **(E)** Representative time trace after a stable NAC•SRP•RNC ternary complex is formed.

5

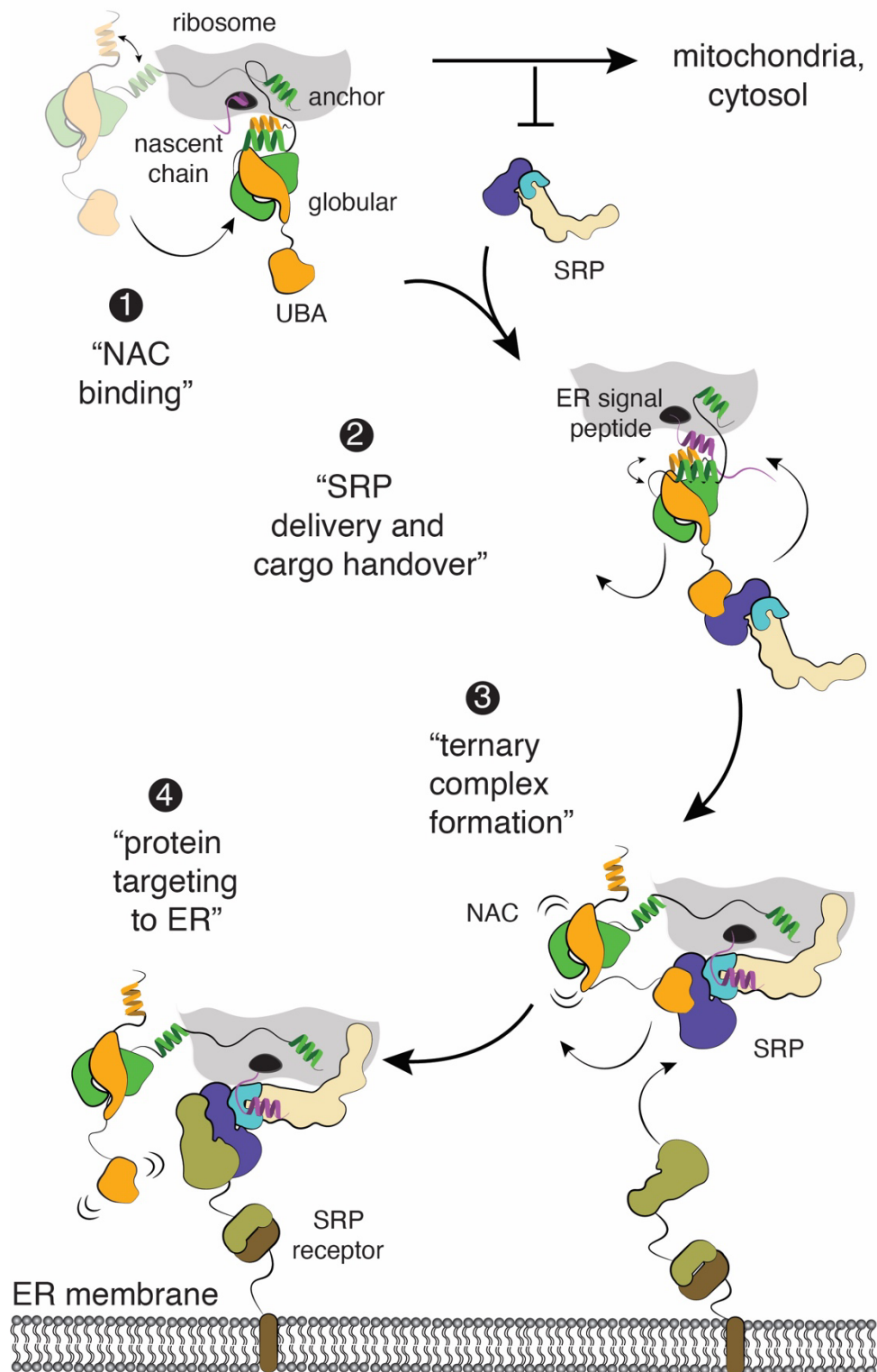


Fig. 5. Model for co-translational signal sequence handover from NAC to SRP during ER-protein targeting.